

Focusing Nanocrystal Size Distributions via Production Control

Michael D. Clark,[†] Sanat K. Kumar,^{*,†} Jonathan S. Owen,[‡] and Emory M. Chan[§]

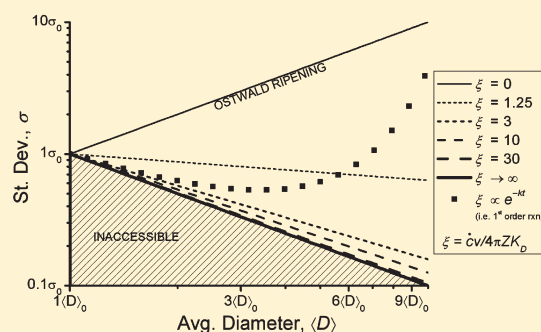
[†]Department of Chemical Engineering and [‡]Department of Chemistry, Columbia University, New York, New York 10027, United States

[§]The Molecular Foundry, Lawrence Berkeley National Laboratory, Berkeley, California 94720, United States

S Supporting Information

ABSTRACT: We present a theoretical description of how continuous monomer production affects the focusing of nanocrystal size distributions in solution. We show that sufficiently high monomer production rates can drive a decrease in the polydispersity even as the average nanocrystal size increases. This is in sharp contrast to Ostwald ripening, where polydispersity increases with mean crystal size. We interpret several experimental nanocrystal studies through our model and show how production-controlled growth promises exquisite control over the size and polydispersity of functional nanocrystals.

KEYWORDS: Nanocrystals, size focusing, theory, chemical production, monodisperse



The synthesis of nanocrystals with narrow size distributions and precisely controlled sizes^{1–7} is important to their use in energy harvesting applications,⁸ light emitting devices,⁹ and biological imaging.^{10,11} In typical nanocrystal syntheses, precursors are added to a reaction mixture where they undergo a chemical reaction that supplies crystallizable “monomers”.^{1–7,12–14} When the monomer concentration reaches a critical level (significantly above its equilibrium solubility), a burst of nucleation occurs. As monomers condense into nuclei and then contribute to nanocrystal growth, their concentration falls below the critical level, ending nucleation.¹⁵

As the monomer concentration is depleted by nanocrystal growth, it approaches the equilibrium solubility and Ostwald ripening begins (also termed as Lifshitz–Slyozov–Wagner growth as described by LSW theory).^{16–18} Under these conditions, smaller nanocrystals dissolve and larger nanocrystals grow by an evaporation–condensation process, causing the cube of the average nanocrystal diameter to grow linearly with time and the polydispersity to increase with increasing average diameter.^{16,17} While the nucleation and Ostwald ripening growth regimes are well-documented features of nanocrystal growth, fewer studies have documented the effect of a slow precursor reaction on the growth kinetics.

Mechanisms that continuously supply monomer to solution can prevent Ostwald ripening and instead improve the monodispersity of the final product. Sugimoto has theoretically shown that under diffusion limited growth high monomer concentrations in solution can force smaller crystals to grow faster than larger ones, thereby causing the nanocrystal size distribution to become narrower with time.¹⁹ Experimental evidence of this behavior was obtained by Wey and Strong in the precipitation of AgBr microcubes.²⁰ Peng et al. found evidence of similar behavior in the synthesis of CdSe and InAs nanocrystals, where “focusing” of the distribution occurred upon injection of

additional precursors during growth.¹⁴ While Sugimoto has qualitatively described the conditions necessary for narrowing, a quantitative description of “size focusing” and its relationship to monomer supply during growth is lacking.

Recently, a number of studies have probed the kinetics of precursor conversion to monomers in nanocrystal synthesis.^{12,21–26} In these studies, precursors slowly convert to monomers as nanocrystals grow. This leads to a pseudosteady state monomer concentration that is controlled by the kinetics of precursor conversion, rather than controlled by the solubility as in Ostwald ripening, and that can influence the narrowing of the size distribution. To quantitatively understand the relationship between monomer production rates and nanocrystal growth, we propose a theoretical model and show that “size focusing” might be extended throughout a synthesis if monomer production can be sustained at sufficient rates during growth^{12,19,27,28} and even more efficiently if the nucleation and monomer production can be decoupled.

Derivation. We begin by using the same governing equations as employed by LSW theory^{16–18} for the rate of diffusion-limited growth of a single nanocrystal of radius R

$$\frac{dR}{dt} = \frac{\nu D}{R} \left((c - c_{\infty}) - \frac{2\gamma c_{\infty}}{RkT} \right) = \frac{K_D}{R^2} \left(\frac{R}{R_c} - 1 \right) \quad (1)$$

The behavior embodied in eq 1 is plotted schematically in Figure 1 (adapted from Sugimoto’s work). Here, $c(t)$ is the solution monomer concentration at time t , c_{∞} is the monomer solubility, D is the monomer diffusivity, ν is the crystal molar volume, and γ is the crystal surface tension. The second equality follows from the definitions that $K_D = (2\gamma\nu^2 c_{\infty} D)/(kT)$ and

Received: January 25, 2011

Revised: March 29, 2011

Published: April 08, 2011

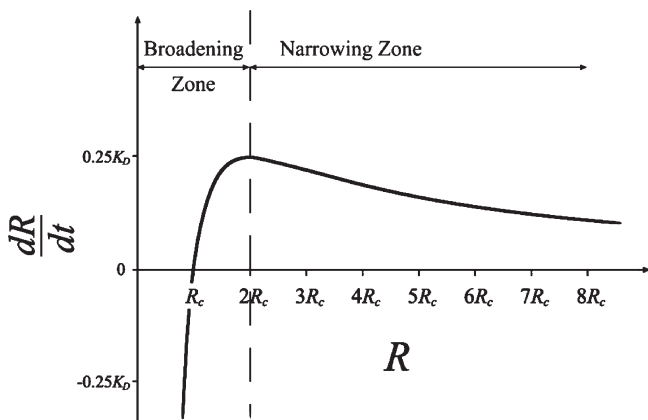


Figure 1. The instantaneous growth rate for a single nanocrystal in a supersaturated monomer solution, as given by Sugimoto.¹⁹ The “broadening zone” and “narrowing zone” correspond to the regions $R < 2R_c$ and $R > 2R_c$.

$R_c = [2\gamma\nu/kT][c_\infty/(c - c_\infty)]$. A central quantity is the “critical” radius, R_c , where $dR/dt|_{R=R_c} = 0$. Crystals with $R > R_c$ will grow in a solution of monomer concentration c , while crystals that are smaller than R_c will shrink. The distribution evolves slowly, becoming increasingly polydisperse with time, and the standard deviation of sizes asymptotically approaches $\sigma = 0.215\langle R \rangle$ at long times and large sizes. Note that the maximum growth rate occurs at $R = 2R_c$.

We augment the LSW derivation by including a production rate of new monomer in the bulk, in an instantaneous “monomer balance” in solution

$$\begin{aligned} \frac{dc}{dt} &= \dot{c} - \int_0^\infty \frac{d}{dt} \left(\frac{4\pi R^3}{3\nu} \right) f(R,t) dR \\ &= \dot{c} - Z \frac{d}{dt} \left(\frac{4\pi \langle R^3 \rangle}{3\nu} \right) \end{aligned} \quad (2)$$

\dot{c} is the rate of new monomer production, $f(R,t)$ is the nanocrystal size distribution function at time t , and $Z = \int_0^\infty f(R,t) dR$ is the number concentration of nanocrystals. We hypothesize that the growth process quickly becomes pseudosteady, that is, $dc/dt \approx 0$. (This assumption holds for any \dot{c} that does not increase with time, as validated in Supporting Information. We show $c(t) \propto \exp(-At^{4/3})$ when \dot{c} is constant.) In this limit, eq 2 then yields

$$\frac{d}{dt} \frac{4\pi \langle R^3 \rangle}{3} = 4\pi K_D \left(\frac{\langle R \rangle}{R_c} - 1 \right) = \frac{\nu \dot{c}}{Z} \quad (3)$$

where the first equality follows from eq 1 (see Supporting Information). We highlight several salient features of eq 3. First, for $\dot{c} = 0$, this yields the LSW result $\langle R \rangle = R_c$. Second, eq 3 expresses the fact that under pseudosteady conditions the rate of production of crystallizable material is equal to the total growth rate of crystals. This simple mass balance result simply reflects our central pseudosteady assumption where the monomer concentration in solution does not change significantly. Third, large values of \dot{c} result in $\langle R \rangle \gg R_c$, and Ostwald ripening does not occur; in this “production-controlled” limit, eq 1 reduces to $dR/dt \propto K_D/R$. Therefore, (a) smaller crystals grow faster than larger ones, and the size distribution becomes more monodisperse as the average size increases, and (b) almost no nanocrystals are

shrinking and the nanocrystal concentration Z is constant. The question is, what experimental conditions define whether production-controlled growth or Ostwald ripening will occur? To establish this transition, we introduce a dimensionless quantity ξ that we call the “size focusing coefficient,” which is the ratio of the monomer production rate per particle to the Ostwald ripening rate

$$\xi = \frac{\nu \dot{c}}{4\pi Z K_D} = \left(\frac{\langle R \rangle}{R_c} - 1 \right) \quad (4)$$

We now consider the size distribution, $f(R,t)$, and how it narrows as $\langle R \rangle$ increases. $f(R,t)$ obeys the continuity equation $\partial f/\partial t = \partial/\partial R [f(dR/dt)]$ ^{16–18,29} in its temporal evolution. The LSW treatment provides an analytical solution for f by assuming it has a time-independent shape $h(R)$ where $f(R,t) = g(t)h(R)$, and thus the solution is obtained by separation of variables.^{16,17}

Since size focusing causes the distribution to become narrower with time, the constant-shape assumption is invalid here and it is not readily possible to derive a general solution to $f(R,t)$ for $\dot{c} > 0$. Instead, we investigate only the evolution of σ , the standard deviation of nanocrystal sizes, through the use of an assumed distribution function, for example, a time-dependent Gaussian.

Employing a Gaussian with average $\langle R \rangle$ and variance σ into the continuity equation yields a nonlinear differential equation whose exact solution is intractable. To gain insights into the behavior of the size distribution function, we employ a regular perturbation analysis in the region near $R = \langle R \rangle$. Therefore, we replace R with $\langle R \rangle(1 + \varepsilon)$ and examine only $\varepsilon \ll 1$, such that terms of higher order than ε are negligible. We thus obtain the following two equations corresponding to the ε^0 and ε^1 terms:

$$-\frac{1}{\sigma} \frac{d\sigma}{dt} = \frac{K_D}{\langle R \rangle^3} (\xi - 1) \quad (5a)$$

$$\frac{d\langle R \rangle}{dt} = \frac{K_D}{\langle R \rangle^2} \left(\xi - \frac{2\sigma^2}{\langle R \rangle^2} (\xi + 1) \right) \quad (5b)$$

We see immediately that σ decreases with time only for $\xi > 1$ [eq 5a], in accordance with previous assertions. Therefore, for any $\xi > 1$ (i.e., $\langle R \rangle > 2R_c$ or at high monomer concentrations), some narrowing occurs, and $\sigma^2/\langle R \rangle^2$ eventually becomes negligible at long times. In this case, eq 5b reduces to eq 3. Combining eqs 5a and 5b at long times for $\xi > 1$ yields the following differential equation

$$\frac{1}{\sigma} \frac{d\sigma}{dt} = \left(\frac{1}{\xi} - 1 \right) \frac{1}{\langle R \rangle} \frac{d\langle R \rangle}{dt} \quad (\forall \xi > 1) \quad (6)$$

For ξ constant or nearly so, we may integrate this equation from an arbitrary time t_0 where the average size and standard deviation are $\langle R \rangle_0$ and σ_0

$$\frac{\sigma(t)}{\sigma_0} = \left(\frac{\langle R \rangle}{\langle R \rangle_0} \right)^{1/\xi - 1} \quad (7)$$

This is our essential result: an equation that details the exact degree of size focusing expected given a monomer production rate embodied in ξ , the size focusing coefficient. This conclusion is in quantitative agreement with the scaling argument of Sugimoto that size focusing only occurs when $\langle R \rangle > 2R_c$ and the single-crystal growth rate decreases with size.^{14,19}

To substantiate the model’s accuracy, eqs 3 and 7 have been compared against numerical simulations of nanocrystal growth

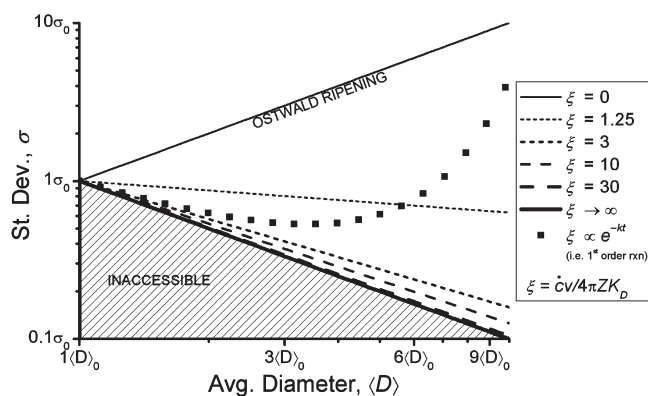


Figure 2. Parametric plot of the steady-state narrowing and broadening of nanocrystals. A NC mixture, initially with average diameter $\langle D \rangle_0$ and standard deviation σ_0 , grows over time to $\langle D \rangle$ and σ with a monomer production rate \dot{c} and size focusing coefficient ξ . $\xi = 0$ results in Ostwald ripening, while $\xi > 1$ causes size focusing. The lines show the degree of focusing for different magnitudes of ξ , approaching $\sigma \propto 1/\langle D \rangle$ as $\xi \rightarrow \infty$. The points represent the size focusing/Ostwald ripening transition when monomer production is due to a 1st-order precursor reaction, thus $\xi(t) = \xi_0 \exp(-kt)$.

based on Mantzaris' population balances.²⁹ Details are noted in the Supporting Information, but the essential result is that for constant ξ , the model equations describe the simulation results to within 2% error on every point and less than 0.3% overall rmsd. Equations 3 and 7 are thus verified by comparison to this numerically exact approach. However, its relevance to experiments is only explored in the next section.

Note that LSW theory includes two treatments of Ostwald ripening, in which either diffusion or the surface adsorption reaction is the rate limiting step. The above derivation was performed for diffusion limited growth, and we note that we also performed the analogous derivation for surface-reaction controlled growth. In this case, in eq 1, D/R is replaced with a reaction constant k_{surf} . For \dot{c} very high in this regime, however, dR/dt no longer has a decreasing tail for large R , and as a result no narrowing can occur. Performing the equivalent Gaussian analysis for f under surface-reaction control, we find $\sigma \propto \langle R \rangle^{1/\xi}$ and no value of ξ causes σ to decrease with time. Therefore, size focusing is only possible at high \dot{c} for diffusion-limited growth.

Comparison with Experiments. There is little systematic data that addresses the role of monomer production kinetics on the polydispersity of nanocrystal sizes. Furthermore, it is challenging to accurately measure nanocrystal concentrations, particularly at small sizes where the error in size measurement leads to large errors (perhaps 30% or more) in the measured nanocrystal volume.²¹ This makes it difficult to obtain experimental proof of size distribution focusing for nanocrystals and hinders experimental validation of our theory. It also underscores the importance of establishing how production rates control size distributions.

For general insights, we can make predictions based on eq 7. Figure 2 plots the diameter-polydispersity relationship at various $\xi \propto \dot{c}$ and a fixed nanocrystal concentration (Z). These plots illustrate the power of controlling the monomer production. In the limit $\dot{c} \approx 0$, Ostwald ripening occurs and the % polydispersity remains constant near 21%, according to LSW theory.^{16,17} In the production-controlled limit, $\dot{c} \rightarrow \infty$, narrowing occurs to its maximum degree with $\sigma \propto 1/\langle R \rangle$ as the crystals grow. We

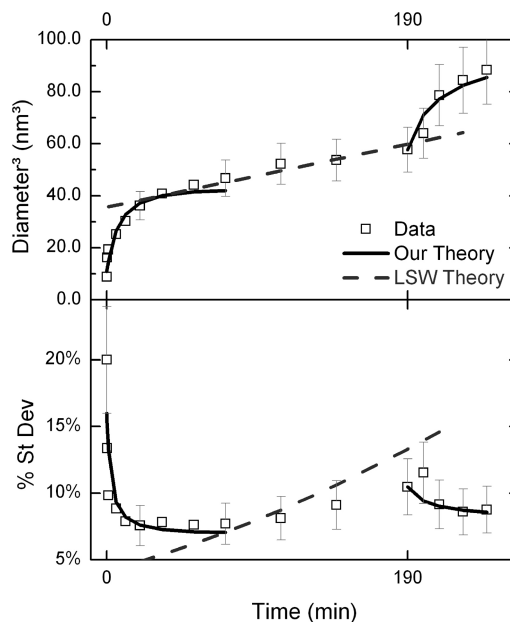


Figure 3. Comparison of theory and data from Peng et al.¹⁴ (Top) Diameter data (squares). (Bottom) % standard deviation data (diamonds). Solid lines represent our model in eqs 3 and 7, dashed lines represent Ostwald ripening by LSW theory.

conducted numerical simulations with various ξ values and found that $\xi = 10^2 - 10^3$ is essentially equivalent to the $\xi \rightarrow \infty$ limit. In this limit, if one begins with nanocrystals at 2.0 ± 0.4 nm (20% polydisperse), then the size distribution will evolve over time to 4.0 ± 0.2 nm (5% polydisperse), then 6.0 ± 0.13 nm (2%), and then 9.0 ± 0.09 nm (1%). While such highly monodisperse crystals have been produced in this manner with micrometer dimensions,^{30,31} our predictions show that monodisperse distributions can be created for nanocrystals smaller than 10 nm, as long as the focusing coefficient is large enough.

We now make a detailed comparison to some of the available experimental data, where narrowing has been observed and the kinetics of precursor conversion to monomer have been studied. In the size-focusing experiments published by Peng et al.,¹⁴ an injection of precursor to the solution during growth led to an immediate drop in polydispersity followed by a slow rebroadening of the distribution. To quantitatively model this data with our theory, we must have measures of the precursor reaction rate, the nanocrystal concentration Z , and the LSW constant K_D . As data for these quantities are unavailable, these are used as fitting parameters. On the basis of our previous observations,²¹ the injection of CdMe_2 and TOPSe precursors leads to a monomer production that follows two competitive pathways: a rapid CdMe_2 thermolysis and a much slower acid-catalyzed TOPSe cleavage.³² To fit the changes in size observed upon injection, we used a single bimolecular rate law with first order kinetics, which effectively captures the reaction kinetics at early times. Our fit yielded $k = 0.0490 \text{ M}^{-1} \text{ s}^{-1}$, $K_D = 6.0 \times 10^{-4} \text{ nm}^3/\text{s}$, and nanocrystal concentrations after the first ($Z_1 = 1.09 \times 10^{-4} \text{ M}$) and second ($Z_2 = 3.83 \times 10^{-5} \text{ M}$) injections (Figure 3).³³

For further validation, we employed Peng's assumption that Ostwald ripening occurs between injections, roughly $t = 75 - 190$ min, as evidenced by the broadening distribution. If this is the case, the diameter should obey the LSW growth law, $\langle R \rangle^3 - \langle R \rangle_0^3 = (4/9)K_D t$, and the polydispersity should follow Wagner's equation VI.9:¹⁷ $\% \sigma = (\% \sigma)_0 \exp[(K_D t)/\langle R \rangle^3]$. These two

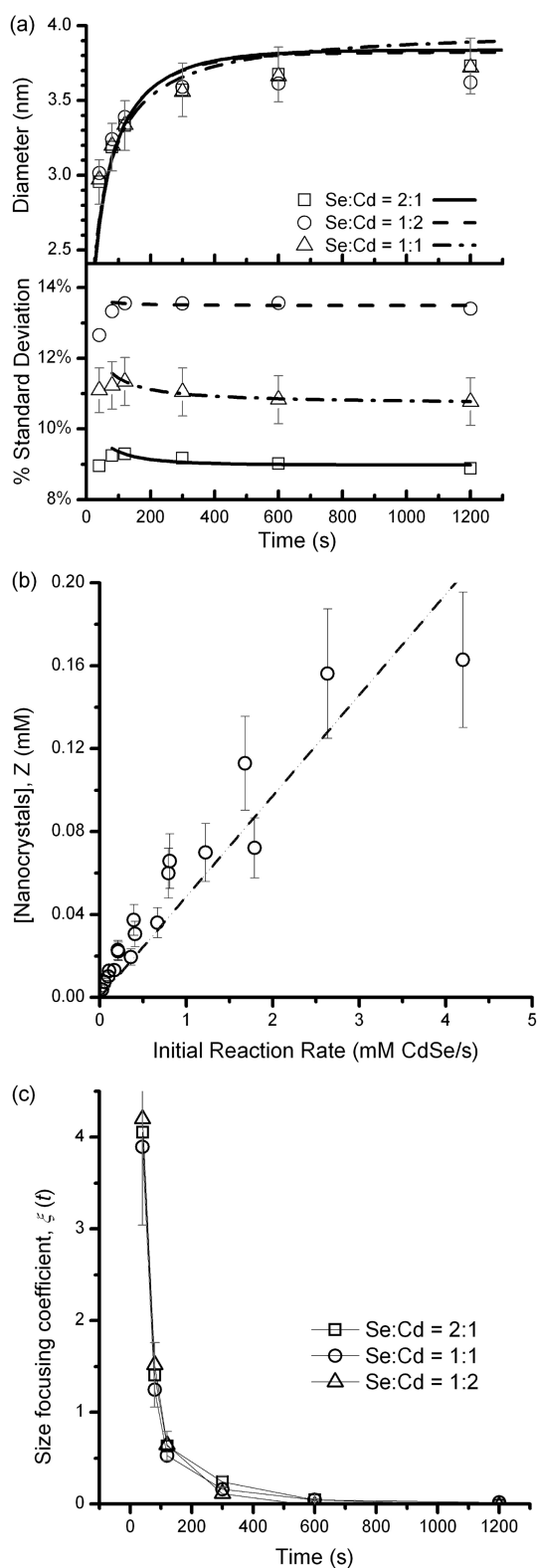


Figure 4. Comparison of theory and data from Chan et al.¹² (a) Experimental data (points) and our model (curves). The three data sets have initial conditions $[\text{Se}]_0/[\text{Cd}]_0 = 74.2/37.1$, $38.4/77.0$, and $74.2/74.2$ mM. (b) Variation of fit parameter Z vs the model's initial reaction rate $k_p[\text{Cd}]_0[\text{Se}]_0$. The solid line in (b) is a linear fit between Z and $k_p[\text{Cd}]_0[\text{Se}]_0$ with zero intercept, as predicted by Sugimoto.³⁶ (c) Variation of the size focusing coefficient, $\xi(t)$, showing no change vs precursor concentrations. All error bars reflect measurement error.

expressions are plotted as dashed lines in Figure 3, using the value of K_D extracted from our fit. The results are in good agreement with the observed changes in diameter and polydispersity,³⁴ reinforcing the value of K_D extracted from this data.

We next turn to a second study of CdSe nanocrystal syntheses by Chan et al.,¹² where eighteen independent CdSe syntheses were conducted with various precursor concentrations. In this study, the concentration of CdSe crystal units was measured directly via UV–vis absorption. With this data, we may develop an accurate expression for \dot{c} from $[\text{CdSe}]$ instead of assuming a chemical mechanism.³⁵ We find that a bimolecular rate expression ($k_p[\text{CdOLA}][\text{TOPSe}]$) provides a more than adequate representation of the kinetic data with $\text{rmsd} = 6.7\%$. Figure 4a plots the experimental data and our model for three representative reactions. $K_D = 9.6 \pm 2.3 \times 10^{-3} \text{ nm}^3/\text{s}$ was fit as a single constant that spans all syntheses that underwent narrowing. Additionally, the variation of the fit parameter Z against the initial reaction rate (Figure 4b) is consistent with Sugimoto's theory of nucleation³⁶ in which Z varies linearly with the initial monomer supply rate, \dot{c}_0 , during nucleation. This lends self-consistency to the assumed kinetics and fit values. We note, however, that because Z varied so closely with \dot{c}_0 across the various reactions, the parameter ξ did not change significantly between syntheses, as shown in Figure 4c. The observed decrease in ξ across all three syntheses arises from the decreasing reaction rate, which is analogous to the first-order reaction kinetics ($\xi \propto e^{-k_p t}$) plotted in Figure 2. This pattern is discussed in more detail below.

Discussion. An interesting aspect of our theory is that the extent of focusing (ξ) depends on both the monomer production rate (\dot{c}) as well as the number of nanocrystals (Z). Although a lack of systematic data makes it difficult to unequivocally verify our prediction, the studies by Chan and Peng are qualitatively consistent with the relationship between \dot{c} , Z , and the focusing coefficient. In the study by Chan et al., \dot{c}_0 and Z are proportional to one another across the range tested (Figure 4b) and no significant differences in the focusing coefficient are observed (Figure 4c). On the other hand, in the study by Peng et al. the second injection of precursors does lead to increased focusing because Z is already fixed at this point in the reaction (i.e., no new nanocrystals are formed) and ξ increases with the increase in \dot{c} .

A number of studies have shown a relationship between the monomer production rate and the number of nuclei. Theoretical predictions published by Sugimoto show that Z can be proportional to the rate of monomer production during homogeneous nucleation (\dot{c}_0)³⁶ A number of experimental studies have provided evidence supporting this correlation, both in the synthesis of micrometer-sized silver halide crystals and in the synthesis of semiconductor nanocrystals.^{21,31,36,37} As a consequence of this relationship, when a single injection of precursors causes homogeneous nucleation and growth, increasing \dot{c} will not effect changes in the initial ξ value ($\xi_0 \propto \dot{c}_0/Z \approx \text{constant}$). Furthermore, because $\dot{c}(t)$ depends on the precursor concentrations, the function \dot{c}/\dot{c}_0 is identical for any initial precursor concentrations. Therefore, even large changes to the precursor concentrations will have little impact on the extent of narrowing, unless they influence K_D . On the other hand, by controlling the nucleation and growth processes independently, one can influence the narrowing of the size distribution during a nanocrystal synthesis.

Seeded growth is one such strategy where nuclei are supplied from an external source, the number concentration of which can be varied over a large range, independent of \dot{c} . These conditions

are effectively obtained in the study by Peng et al., where the second precursor injection does not effect nucleation; thus Z is established prior to the second injection and the new ξ may be adjusted through the volume of the injection. Likewise, under conditions where nanocrystal precursors are mixed at room temperature and slowly heated, nucleation occurs at a lower temperature than growth, potentially leading to higher pseudosteady state supersaturation.³⁸

Conclusion. We have developed a theory of size distribution focusing of nanocrystals that includes a rate at which monomers are produced in the reaction medium over time. Using our model we show how size distributions of nanocrystals can narrow or broaden depending on the rate of the monomer production and the number of nanocrystals. We further suggest that seeded nanocrystal growth reactions are likely to give rise to synthetic methods where size focusing can be best controlled. Under these conditions the number of nanocrystals and the monomer production rate can be independently tuned to optimize size focusing and permit the *a priori* design of procedures that produce nanocrystals of a desired size and polydispersity.

■ ASSOCIATED CONTENT

S Supporting Information. Additional information. This material is available free of charge via the Internet at <http://pubs.acs.org>.

■ AUTHOR INFORMATION

Corresponding Author

*E-mail: sk2794@columbia.edu.

■ ACKNOWLEDGMENT

We acknowledge financial support from the National Science Foundation. Portions of this work were performed at the Molecular Foundry, Lawrence Berkeley National Laboratory, and were supported by the Office of Science, Office of Basic Energy Sciences, of the U.S. Department of Energy, under Contract No. DE-AC02-78105SCH11231. M.D.C. and S.K.K. conducted the derivation, numerical studies, and all data fits. J.S.O. and E.M.C. provided fundamental concepts and experimental data. M.D.C., S.K.K., and J.S.O. wrote the paper.

■ REFERENCES

- (1) Brust, M.; Walker, M.; Bethell, D.; Schiffrin, D. J.; Whyman, R. *J. Chem. Soc., Chem. Commun.* **1994**, 7, 801–802.
- (2) Lin, X. M.; Sorensen, C. M.; Klabunde, K. J. *Chem. Mater.* **1999**, *11* (2), 198–202.
- (3) Lin, X. M.; Sorensen, C. M.; Klabunde, K. J. *J. Nanopart. Res.* **2000**, *2*, 157–164.
- (4) Murray, C. B.; Norris, D. J.; Bawendi, M. G. *J. Am. Chem. Soc.* **1993**, *115* (19), 8706–8715.
- (5) Prasad, B. L. V.; Stoeva, S. I.; Sorensen, C. M.; Klabunde, K. J. *Langmuir* **2002**, *18* (20), 7515–7520.
- (6) Prasad, B. L. V.; Stoeva, S. I.; Sorensen, C. M.; Klabunde, K. J. *Chem. Mater.* **2003**, *15* (4), 935–942.
- (7) Samia, A. C. S.; Schlueter, J. A.; Jiang, J. S.; Bader, S. D.; Qin, C. J.; Lin, X. M. *Chem. Mater.* **2006**, *18* (22), 5203–5212.
- (8) Huynh, W. U.; Dittmer, J. J.; Alivisatos, A. P. *Science* **2002**, *295* (5564), 2425–2427.
- (9) Colvin, V. L.; Schlamp, M. C.; Alivisatos, A. P. *Nature* **1994**, *370* (6488), 354–357.
- (10) Smith, A. M.; Ruan, G.; Rhyner, M. N.; Nie, S. M. *Ann. Biomed. Eng.* **2006**, *34* (1), 3–14.
- (11) Michalet, X.; Pinaud, F. F.; Bentolila, L. A.; Tsay, J. M.; Doose, S.; Li, J. J.; Sundaresan, G.; Wu, A. M.; Gambhir, S. S.; Weiss, S. *Science* **2005**, *307* (5709), 538–544.
- (12) Chan, E. M.; Xu, C. X.; Mao, A. W.; Han, G.; Owen, J. S.; Cohen, B. E.; Milliron, D. J. *Nano Lett.* **2010**, *10* (5), 1874–1885.
- (13) Dushkin, C. D.; Saita, S.; Yoshie, K.; Yamaguchi, Y. *Adv. Colloid Interface Sci.* **2000**, *88* (1–2), 37–78.
- (14) Peng, X. G.; Wickham, J.; Alivisatos, A. P. *J. Am. Chem. Soc.* **1998**, *120* (21), 5343–5344.
- (15) Lamer, V. K.; Dinegar, R. H. *J. Am. Chem. Soc.* **1950**, *72* (11), 4847–4854.
- (16) Lifshitz, I. M.; Slyozov, V. V. *J. Phys. Chem. Solids* **1961**, *19* (1–2), 35–50.
- (17) Wagner, C. Z. *Elektrochem.* **1961**, *65* (7–8), 581–591.
- (18) Kahlweit, M. *Adv. Colloid Interface Sci.* **1975**, *5* (1), 1–35.
- (19) Sugimoto, T. *Adv. Colloid Interface Sci.* **1987**, *28* (1), 65–108.
- (20) Wey, J. S.; Strong, R. W. *Photogr. Sci. Eng.* **1977**, *21* (5), 248–252.
- (21) Owen, J. S.; Chan, E. M.; Liu, H.; Alivisatos, A. P. *J. Am. Chem. Soc.* **2010**, *132* (51), 18206–18213.
- (22) Allen, P. M.; Walker, B. J.; Bawendi, M. G. *Angew. Chem., Int. Ed.* **2010**, *49* (4), 760–762.
- (23) Joo, J.; Pietryga, J. M.; McGuire, J. A.; Jeon, S. H.; Williams, D. J.; Wang, H. L.; Klimov, V. I. *J. Am. Chem. Soc.* **2009**, *131* (30), 10620–10628.
- (24) Liu, H. T.; Owen, J. S.; Alivisatos, A. P. *J. Am. Chem. Soc.* **2007**, *129* (2), 305–312.
- (25) Steckel, J. S.; Yen, B. K. H.; Oertel, D. C.; Bawendi, M. G. *J. Am. Chem. Soc.* **2006**, *128* (40), 13032–13033.
- (26) Baek, J.; Allen, P. M.; Bawendi, M. G.; Jensen, K. F. *Angew. Chem., Int. Ed.* **2011**, *50* (3), 627–630.
- (27) Reiss, H. J. *Chem. Phys.* **1951**, *19* (4), 482–487.
- (28) Yin, Y.; Alivisatos, A. P. *Nature* **2005**, *437* (7059), 664–670.
- (29) Mantzaris, N. V. *Chem. Eng. Sci.* **2005**, *60* (17), 4749–4770.
- (30) Kanie, K.; Sugimoto, T. *J. Am. Chem. Soc.* **2003**, *125* (35), 10518–10519.
- (31) Sugimoto, T.; Shiba, F.; Sekiguchi, T.; Itoh, H. *Colloids Surf., A* **2000**, *164* (2–3), 183–203.
- (32) The bulk concentration in solution never reaches a large enough value to cause additional nucleation.
- (33) Peng et al. noted that the number of particles in their synthesis stayed constant during “focusing” events and decreased during “defocusing”, presumably due to the Ostwald ripening process in which nanocrystal concentration decreases with time.
- (34) The deviation of our fit from the observed polydispersity during the Ostwald ripening period may be caused by a background acid catalyzed TOPSe cleavage, which maintains a nonzero monomer production.
- (35) We fit the generation of CdSe to a general rate law, in which the reaction rate constant of the exponents of the two precursors were permitted to float. All reaction data were used in the fit of the three parameters.
- (36) Sugimoto, T. *J. Colloid Interface Sci.* **1992**, *150* (1), 208–225.
- (37) Sugimoto, T.; Shiba, F. *Colloids Surf., A* **2000**, *164* (2–3), 205–215.
- (38) The pseudosteady state supersaturation in so-called “heating-up” methods will depend on the relative response of the nucleation and precursor conversion rate to increasing temperature. Furthermore, the relationship between concentration and the critical radius R_c depends strongly on temperature. For examples of the heating-up method see: (a) Park, J.; et al. *Angew. Chem., Int. Ed.* **2007**, *46*, 4630–4660. (b) Yang, Y. A.; et al. *Angew. Chem., Int. Ed.* **2005**, *44*, 6712–6715. (c) Chen, Y.; Johnson, E.; Peng, X. *J. Am. Chem. Soc.* **2007**, *129*, 10937–10947.